

# A CBIR SYSTEM FOR LOCATING AND RETRIEVING PIGMENT NETWORK IN DERMOSCOPY IMAGES USING DERMOSCOPY INTEREST POINT DETECTION

Ardalan Benam<sup>1</sup>, Mark S. Drew<sup>1</sup>, M. Stella Atkins<sup>1</sup>

<sup>1</sup>School of Computing Science, Simon Fraser University, Burnaby, Canada

## ABSTRACT

We designed a content based image retrieval (CBIR) system for dermoscopic images focusing on images with pigment networks. The system locates and matches a query image that has a pigment network with the most similar images containing pigment networks in a database of dermoscopic images. Dermoscopy interest points in the query image are detected and a vector of 128 features is extracted as the descriptor from each keypoint. Then, the descriptors are matched according to our matching algorithm to similar features arising in the database images. This leads to a meaningful matching as we are matching similar dermoscopy structures with each other. The performance of the system has been tested on more than 1000 images. Results show that our system will locate and retrieve similar images with pigment networks, with accuracy > 80.7%. This system can help physicians in diagnosis as they are shown similar looking dermoscopy images with known pathology.

*Index Terms*— CBIR, Interest point detection, dermoscopic image, pigment network, pigmented skin lesion

## 1. INTRODUCTION

Skin cancer is one of the most common of all cancers and its worldwide mortality rate is increasing [1]. Malignant melanoma can be deadly; however, if it is caught in an early stage, it can be often cured. Dermoscopy is a non-invasive diagnostic imaging technique for in vivo inspection of epidermis to the papillary dermis. Dermoscopy imaging with a polarizer or a skin surface gel removes the reflection of light and helps the penetration of light into epidermis. Studies have shown that dermoscopy improves diagnosis accuracy in comparison with clinical diagnosis with the naked eye; however, the success is directly dependent on the experience of the observer. Consequently, several dermoscopy diagnostic algorithms have been introduced in order to increase the accuracy of inexperienced doctors. The ABCD rule, 7-point checklist and 3-point checklist are examples of these methods [2]. Recent developments in computer vision have motivated research on detection and implementation of algorithms that mimic these clinical algorithms, as reviewed by Celebi *et al.* in [3]. Moreover, a review by Rosado *et al.* [4] on computer aided diagnosis (CAD) systems of

dermoscopic images shows that the results achieved by the computer are statistically the same as human diagnosis. However, another study [5] shows that the second diagnosis is not always welcomed by physicians when it does not match their own initial diagnosis. In fact, the study showed that only 24% of physicians changed their decision when they encounter a second different diagnosis proposed by the CAD system.

Another approach using CAD systems is to assist the physicians to a precise diagnosis instead of giving a crisp second decision. Doi [6] believed that providing physicians with similar looking lesions with a confirmed pathology diagnosis would efficiently assist the physician to a more confident diagnostic decision. This concept is known as Content-Based Image Retrieval (CBIR) in computer vision. Retrieving similar looking cases can provide a diagnostic support environment rather than a single second diagnosis.

Chung *et al.* developed one of the very early basic concepts of image retrieval in dermoscopy. They designed a system allowing the user to query the database using feature attribute values — but the user had to input the feature values and then a web-based data browser retrieved all of the images with those feature values [7]. Rahman *et al.* introduced an image retrieval system based on the contents on the query. In this algorithm the lesion was segmented and dermoscopic features were extracted. Then the similarity between different images was found by comparing their feature vectors using the Euclidean and Bhattacharyya metrics [8]. Dorileo *et al.* introduced CBIR to dermatological lesions by using color histogram and texture features for similar-image retrieval [9]. A modern approach is using deep learning to classify images according to their features [10], but many thousands of labelled images would be required to train the system.

However, a closer inspection of the published literature in dermoscopy CBIR shows that they all suffer from the downside of the so-called semantic gap. In all of the proposed systems the traditional approach is taken, i.e. a feature vector is extracted from the query image and the most similar images according to distance metrics are retrieved. This approach is different from what humans do in order to determine similarity. Instead, a more meaningful approach can be taken, which is to match the low level characteristics such as blobs, dots, streaks etc. Locating and matching the similar looking dermoscopic interest points (DIP) will lead to a more meaningful image retrieval. The concept of DIP was

first introduced by Zhou *et al.* in [12]. They proposed using blob detectors and a curvilinear structure detector for finding the meaningful points with important dermoscopic information.

Pigment networks (PNs) are one of the most common and important structures in dermoscopy images. Pigment networks can be defined as a set of pale blobs with dark borders attached to each other in a rectilinear pattern. An alternative method to retrieve images with pigment networks could be to perform image processing on the images to detect PN, such as described by Sadeghi *et al.* [11]. However, this system would only detect the presence or absence of the PNs, and would not be capable of retrieving similarly colored lesions. We designed a CBIR system which is focused on locating and retrieving images with PNs using luminance and color components for each keypoint detected.

## 2. METHOD

We begin by detecting blob structures which occur at the center of PNs. We based our blob detection on SIFT [13] and SURF [14], which are the most popular interest point detectors that focus on blob and corner detection.

Before analyzing the image, histogram equalization was performed as a preprocessing step; this gave PNs a better contrast so that they could be detected easily by the blob detector.

### 2.1. Blob detection

We took the same approach as SURF for blob detection. Here we adapt that seminal method to dermoscopy images in particular. Our implementation, along with keying the method to dermoscopy images, goes on to also add color information in a novel approach. The blue channel of the RGB image was used as it contains the most contrast in dermoscopic images. Then, the determinant of Hessian matrix is calculated to locate the interest point location and scale. The Hessian matrix  $\mathcal{H}(\vec{x}, \sigma)$  when given a point  $\vec{x} = (x, y)$  and scale  $\sigma$  is defined as bellow

$$\mathcal{H}(\vec{x}, \sigma) = \begin{bmatrix} L_{xx}(\vec{x}, \sigma) & L_{xy}(\vec{x}, \sigma) \\ L_{xy}(\vec{x}, \sigma) & L_{yy}(\vec{x}, \sigma) \end{bmatrix}. \quad (1)$$

In the equation above  $L_{xx}(\vec{x}, \sigma)$  refers to the convolution of the image  $I$  with the second order Gaussian derivative  $\frac{\delta^2}{\delta x^2} g(\sigma)$ , and similarly for  $L_{xy}$  and  $L_{yy}$ . SURF detector approximates the Laplacian of Gaussian with box filters (Fig.1), which are efficiently calculated using the concept of integral image. These approximations are referred to  $D_{xx}$ ,  $D_{xy}$ , and  $D_{yy}$ . The filter response is then calculated by the approximate determinant of the Hessian matrix as  $\det(\mathcal{H}_{approx}) = D_{xx}D_{yy} - (0.9D_{xy})^2$ . Here, 0.9 is to balance the approximation of the filter. Moreover, the computation of the scale space has been done using the integral images and box filters. Given an image  $I$ , the integral image  $I_{\Sigma}(x, y)$  is defined as follows:

$$I_{\Sigma}(x, y) = \sum_{i=0}^{x-1} \sum_{j=0}^{y-1} I(i, j). \quad (2)$$

Now in order to build the scale-space we need to convolve Gaussian kernels of increasing size with the original image. Since we are using integral images the processing time is invariant to the size of the kernel. Therefore, we can build each image layer by filtering the original image with increasing masks (e.g. 9x9, 15x15, 21x21). This leads to calculating multiple layers of scale space simultaneously.

Then, non-maximal suppression is applied in order to find the candidate points. Therefore, all of the pixels in scale-space are compared with their 26 neighbors, that is 9 in each scale above or below and 8 at the same scale.

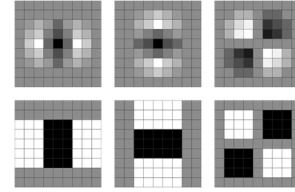


**Fig. 1.** First row: Gaussian partial derivative in x-, y-, and xy- direction. Second Row: approximated filters using box filters.

As the next step the Hessian determinant is interpolated in both scale and space. The final step is thresholding the responses for a precise blob detector.

Using this blob detector on an image with PNs, most of the network centers can be detected. Fig. 2 shows an example of this keypoint detection.

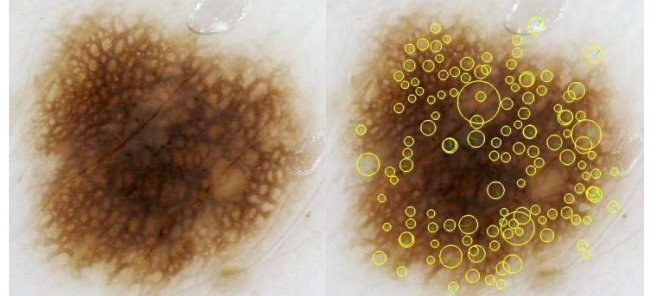


**Fig. 2.** Left image: a sample pigment network. Right image: the results of blob detection on the pigment network (highlighted in yellow). Most of the pigment network's holes have been detected

### 2.2. Descriptor

Once the location of a DIP is determined, we have to find an orientation for the interest point in order to make our result rotation invariant. SURF calculates the orientation by computing the Haar-wavelet responses with the help of integral images and we have taken the same approach. After the orientation of the keypoint is determined, a square with the size of 20s is formed along the direction of the

calculated dominant orientation. This square is divided uniformly into  $4 \times 4$  sub-regions. Then 4 features are calculated in each region. In each sub-region the Haar-wavelet is calculated. Moreover, in each sub-region, Haar-wavelets of size  $2s$  are calculated that provides 25 wavelet responses for each subregion. We annotate the wavelet responses in the horizontal and vertical direction by  $d_x$  and  $d_y$  respectively. Also, we assume that  $|d_x|$  and  $|d_y|$  are the absolute value of the Haar-wavelets calculated in each horizontal and vertical direction, respectively. Therefore, the feature vector for each sub-region is  $v = (\sum d_x, \sum d_y, \sum |d_x|, \sum |d_y|)$ . This provides a vector of size 64 for each keypoint.

### 2.3 Color

Color plays an important role in dermoscopy image analysis. For instance, the profile of a dark globule or dot might be the same as the profile of the holes of pigment network and color is one of the important components in differentiating them. Also, color helps to retrieve more similar looking pigments and helps disambiguate visual similarity. Therefore, we have included color in our descriptor. The size of the dermoscopic structure that is detected by our detector is proportional to the scale of the keypoint. Therefore, as the extraction of color information from all of the structure's region is desired, we calculate the color histogram of a circle with radius  $7s$  centered at the keypoint. We calculate the three dimensional color histogram in the interest region in channels R, G, and B (4 bins in each dimension). This results in a vector of length 64 which records the color distribution of the region. As the last step we normalize the color component and concatenate it to the intensity component. This results in a descriptor of length 128.

### 2.4. Matching

Traditionally, in most CBIR systems, in order to find a match for a keypoint, the descriptor of that keypoint is compared to other descriptors by using a distance metric (e.g. Euclidean distance). Then the keypoint with the least distance is declared a match.

However, we propose that this approach does not work for matching pigment networks. As most of the pigment networks' holes are the same we would not be able to find correct matches by deploying the traditional method. For if we do so, we encounter cases where many keypoints in one image are matched to a single keypoint in the other image (see Fig.3.)

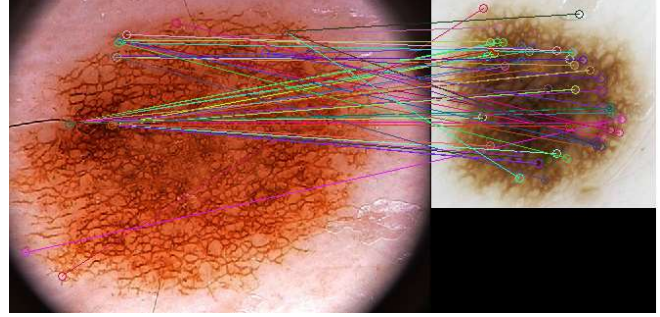


**Fig. 3.** Error in matching the keypoints when using the traditional approach. Most of the keypoints in the right image are matched to a single keypoint in the left image.

To solve this problem, we calculate the distance of a keypoint in one image to all of the keypoints in the second image, using the Euclidean distance metric and store these distances in a matrix. Once we have done this for all of the keypoints we search for the minimum distance amongst all of the distances in the matrix, which forms the most promising match amongst all of the possible matches. We then remove those points from our matrix so that they can't be matched to any other point. We continue until all of the keypoints are matched, as shown in Fig. 4.

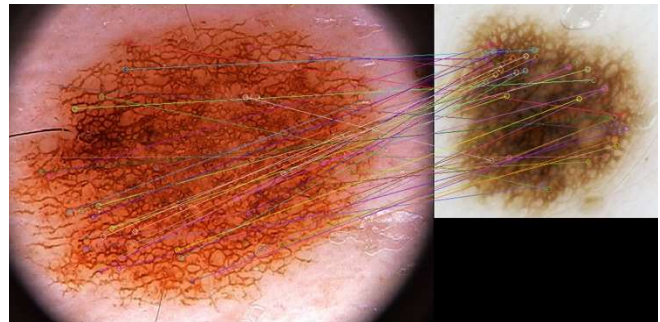


**Fig. 4.** Matching with new algorithm. We observe that many of the holes are matched to other holes.

After matching all of the keypoints of one image to the other, we calculate the similarity of two images by taking the average distance of all the matches.

## 3. EVALUATION, RESULTS AND DISCUSSION

This CBIR system was evaluated by using 1011 labelled images from the IAD Atlas [15] (380 with typical PN). To evaluate the system, all of the images in the database were fed in turn into the system as a query image. When the query image contains a PN, the precision is defined as the average number of images with a PN in the first 9 retrieved images, averaged over every query image. The same definition for

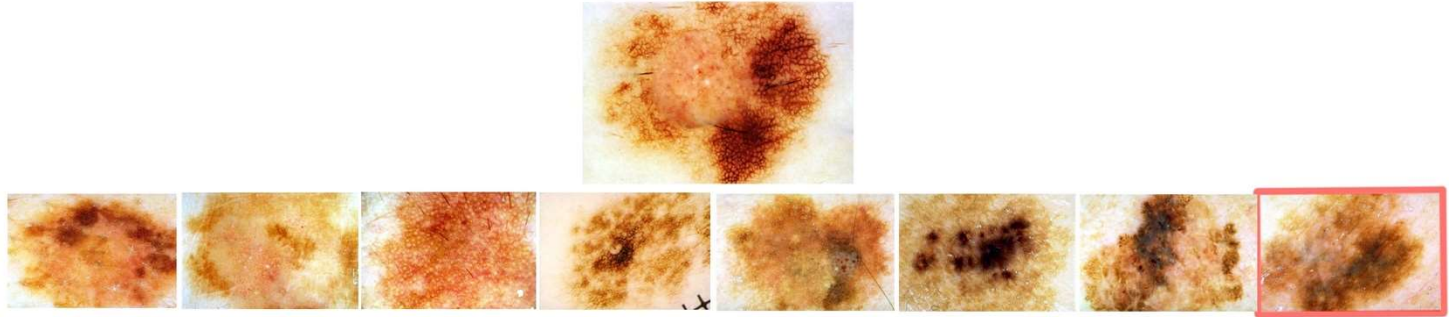


**Fig. 5.** Top shows the query image with pigment network highly visible on the right side. Second row are the retrieved images sorted L to R based on their similarity – all the images contain pigment network except the 8th one with red borders.

precision holds for when the query image does not contain a PN. The table below shows the precision for each case:

	Precision
Query contains PN	75.4%
Query does not contain PN	81.2%

An example of a query image with PN and the first eight retrieved images is given in Fig. 5. Only the eighth image (shown with a red border) does not contain a PN. The precision of this individual case is 88.9%. This example shows that despite the very different background color of the skin, only PNs of similar color are retrieved. This is one of the advantages of this system over other CBIR systems with global features. Also, all of the images retrieved except the eighth one (with red border) contain a PN. If we investigate this case further, we find that the presence of artifacts and sun damage pigmentation causes this image to show up as a false positive. Artifacts like hair, air bubbles, skin damage etc. are also detected by this algorithm and sometimes interfere with our results.

Our method for retrieving PNs is visually acceptable; unfortunately, no other CBIR systems have been evaluated, so no comparison with other methods is possible.

#### 4. CONCLUSION

We implemented a CBIR approach toward dermoscopic CAD systems focusing on PNs. The main goal of this system is to locate and retrieve images with similar PNs. This is a consequential CBIR system as it matches meaningful interest points. Since most of the keypoints are always on the inside of the lesion, the color of the skin does not play a significant role in the CBIR result, unlike in traditional CBIR methods. To the best of our knowledge there are no other published results in CBIR dermoscopy to be compared to our methods.

Future work includes expanding this approach to other clinical dermoscopic structures and asking dermatologists to evaluate the CBIR system for usefulness. Providing doctors with a set of known-diagnosis images that are visually similar to the unknown case will help them make more confident diagnoses.

#### 5. REFERENCES

- [1] M.B. Lens, Dawes, "Global perspectives of contemporary epidemiological trends of cutaneous malignant melanoma," *Br. J. Dermatol.*, 2004, 150, 179-185.
- [2] G. Argenziano, G. Fabbrocini, P. Carli, V. De Giorgi, E. Sammarco, "Epiluminescence microscopy for the diagnosis of doubtful melanocytic skin lesions. Comparison of the ABCD rule of dermoscopy and a new 7-point checklist based on pattern analysis," *Arch. Dermatol.*, 1998, 134, 1563-1570.
- [3] M. E. Celebi, H. A. Kingravi, B. Uddin, H. Iyatomi, Y. A. Aslandogan, W. V. Stoecker, and R. H. Moss, "A Methodological approach to the classification of dermoscopy images," *Computerized Medical Imaging and Graphics*, vol. 31, pp. 362-373, Sep. 2007.
- [4] B. Rosado, S. Menzies, A. Harbauer, H. Pehamberger, K. Wolff, M. Binder, and H. Kittler, "Accuracy of computer diagnosis of melanoma: a quantitative meta-analysis," *Arch. Dermatol.*, vol. 139, no. 3, pp. 361-7, discussion 366, Mar. 2003.
- [5] S. Dreiseitl and M. Binder, "Do physicians value decision support? A look at the effect of decision support systems on physician opinion.," *Artificial Intelligence in Medicine*, vol. 33, pp. 25-30, Jan. 2005.
- [6] K. Doi, "Computer-Aided diagnosis in medical imaging: historical review, current status and future potential," *Computerized Medical Imaging and Graphics*, vol. 31, pp. 198-211, Mar. 2007.
- [7] S. M. Chung and Q. Wang, "Content-based Retrieval and Data Mining of a skin cancer image database," in *Proc. OF IEEE Int. Conf. Information Tech. Coding & Computing*, vol. 1, pp. 611-615, Apr. 2001.
- [8] M. M. Rahman, B. C. Desai, and P. Bhattacharya, "Image retrieval-based decision support system for dermoscopic images," in *Proc. 19th IEEE International Symposium on Computer-Based Medical Systems*, 2006, pp. 285-290.
- [9] E. A. G. Dorileo, M. A. C. Frade, A. M. F. Roselino, R. M. Rangayyan, and P. M. Azevedo-Marques, "Color image processing and content-based image retrieval techniques for the analysis of dermatological lesions," in *Proc. 30th Annual International Conference of the IEEE Engineering in Medicine and Biology Society*, 2008, pp. 1230-1233.
- [10] J. Premalatha, K.S. Ravichandran, "Novel Approaches for Diagnosing Melanoma Skin Lesions through Supervised and Deep Learning Algorithms," *J. Med. Syst.* **2016**, 40, 96.
- [11] M. Sadeghi, M. Razmara, T.K. Lee and M.S. Atkins, "A novel method for detection of pigment network in dermoscopic images using graphs," *Computerized Medical Imaging and Graphics*, 35(2011), pp. 137-143, May 2011.
- [12] H. Zhou, M. Chen, J.M. Rehg, "Dermoscopic interest point detector and descriptor," *Biomedical Imaging: From Nano to Macro, 2009. ISBI'09.*, IEEE International Symposium on; IEEE. 2009. pp. 1318-1321.
- [13] David G. Lowe, "Distinctive image features from scale-invariant keypoints," *Intl. J. of Computer Vision*, vol. 60, pp. 91-110, 2004.
- [14] H. Bay, T. Tuytelaars, and L.V. Gool, "Surf: Speeded up robust features," in *Eur. Conf. on Computer Vision (ECCV)*, 2006, pp. 404-417.
- [15] G. Argenziano : *Interactive Atlas of Dermoscopy (Book and CD-ROM)*. Edra medical publishing and new media, Milan (2000)